Experimental Investigation of Stochastic Jumps during Crack Initiation and Growth in IN718

Joel Lindsay*, Stefanos Papanikolaou*♦, Terence Musho*+

* Department of Mechanical & Aerospace Engineering, West Virginia University, 395 Evansdale Drive, Morgantown, WV, 26506-6070

♦ Department of Physics & Astronomy, West Virginia University, 135 Willey St., Morgantown, WV, 26506

+ Corresponding Author

Abstract:

This study investigates the statistical significance of crack jump noise in Inconel 718 (IN718) for several different loading conditions. A direct current potential drop (DCPD) method is used to experimentally measure *in-situ* the crack length. Data is collected for six different peak loads at R=0.15 for a statistically significant number of trails. FEA-derived calibration curves relate measured potential to crack length. We determine that the mean crack length *jumps*, over subsequent cycles, increased with loading, the range of the crack length jump distributions decreases with increasing load, while the noise has a non-zero mean distribution. Findings from this study suggest that crack length jumps are not random events but contain statistical features that can potentially be used with machine learning approaches to better understand fatigue progression in Ni-based superalloys.

Keywords: Crack Propagation; DCPD; Inconel 718; Fatigue

Introduction:

With the recent move to reduce the carbon emissions across many counties and the constant goal of reducing operation cost, gas turbine efficiency can achieve both goals and has been increasing steadily over the past 50 years [1]. One of the methods that have been employed to increase the gas turbine efficiency is to have turbines operate at higher temperatures [2]. However, higher temperatures require new materials and alloys, as well as better understanding of the basic physics that may drive materials informatics [3]. Regarding mechanical response, a better understanding of this physics in various materials has coincided with the development of new predictive models for failure mechanisms. A common superalloy used in the disk of turbines is Inconel 718 (IN718), a nickel-based alloy that is designed to withstand extreme temperatures under high creep load conditions. The main constitutive elements in this type of superalloys are nickel, cobalt, and iron with precisely prescribed precipitate-hardened microstructure that provides high strength, high operating temperatures, as well as creep and oxidation resistance. It is a combination

of constitutive elements and microstructure but more so the microstructure that impedes and govern the crack initiation and growth in this material. However, structural health monitoring has been typically limited in qualitative assessments of isolated microstructural observations. Beyond the study of averages, a fundamental understanding of crack initiation and growth, as well as structural health assessment, requires new approaches that focus on connecting experiments and advanced simulations in the statistical frontier. In this study, the objective is to monitor the dynamics of crack initiation and growth in an IN718 sample under monotonic low-cycle fatigue loading and use it towards a history-informed, as well as statistically-informed assessment of structural health.. More specifically, the focus in this work is to capture the statistical variation of the magnitude of crack length growth versus cycle number during initiation and growth stages.

In this study, IN718 has been selected as the material of focus due to its polycrystalline nature and wide application in contemporary turbines [4]. IN718 has a wide range of operating temperatures from -423°F to 1300°F while maintaining strength, good mechanical properties of weldability, and resistance to cracks commonly caused by welding [5]. The key to IN718's performance is the compositional complexity of 15+ constitutive elements including titanium, cobalt, niobium, etc., as well as a production processing stage which optimizes the precipitate hardening capacity of the alloy [5]. The important aspect of IN718 is the strengthening phases of the microstructure. The primary strengthening phase is the γ" phase, which is a metastable phase, with the δ phase being the thermodynamically favorable phase. Since the γ" phase is not thermodynamically favorable, the over-aging cooling rates must be precisely controlled: During this non-equilibrium cooling process, the γ" phase partially orders in disk-shaped precipitates that are coherent with the γ phase. The origin of the ordering lies into the emergence of coherent strains from the lattice distortion of the precipitate formation [6]. In addition to γ", there are also secondary phases γ' and γ present within IN718. The γ' phase also plays an important role as a strengthening phase in IN718, but to a lesser degree than γ". The γ" phase is on the order of four times larger than the γ' phases [7]. The γ' are often found as a fine dispersion of spherical particles, which are also coherent with the γ phase. It is interesting to point out that the coherency of these precipitate phases should potentially be relevant in the origin and magnitude of crack length jumps as fatigue progresses.

The main focus of this work is the crack length during initiation and growth. For this purpose, there are several experimental methods: The simplest method involves the use of a high resolution optical microscope, which

is typically limited to distinguishing up to submicron features [8]. Another common method is the use of an optical microscope in conjunction with another measurement method such as a direct-current potential drop (DCPD) method [9]. Other approaches include *in-situ* SEM of crack growth; however, this approach requires special equipment that integrates a field emission gun with a tensile testing apparatus [10]. Digital Image Correlation (DIC) measurements can also take *in-situ* measurements of crack growth [11, 12] along with the added benefit of being able to measure the strain field of the specimen [13]. The measurement method selected for this study is the ASTM-recommended direct current potential drop (DCPD) method [14] to measure *in-situ* short crack growth in low cycle fatigue crack-growth.

Experimental Method

The experimental method employed for this study is based on the combination of the DCPD method and fatigue loading of a statistically significant (>100) number of IN718 samples in a hydraulic MTS load frame. We employ the ASTM compact specimen standard testing procedure with a custom specimen geometry. The test specimens were not run to failure but were stopped prior to the ultimate fracture crack growth point. Samples were initiated with an EDM in the absence of a crack initiation procedure to capture the crack initiation event and the later stages of crack propagation.

Test Specimen Design

Following the ASTM compact specimen [14] design specification, a custom test specimen was designed based on a plane strain based IN718 material. The design is a 76.2mm x 36.63mm simple rectangle of plate Inconel 718 with two holes for mounting the specimen. A schematic of the design is illustrated in Figure 1A. Along with the two mounting holes, a small 10mm slit was cut using electrical discharge machining (EDM) with a width of 0.16mm. The EDM cut serves the purpose of acting as an initial crack in the material. The tip of this initial crack is rounded with a radius equivalent to the EDM wire or 0.08mm. In providing electrical continuity without introducing secondary materials nickel-chromium wires with a diameter of 0.4mm were spot-welded to the samples. Care was taken to spot-weld the wires in the same position of either side of the EDM. These wires closest to the EDM cut serve as the voltage probes. A larger gauge nickel-chromium wire with a diameter of 1.0mm was spot welded across the full specimen as current leads 15mm above and below the EDM cut. This wire placement provides a uniform potential across the specimen. This is analogous to the original DCPD experiment setup by H. Johnson who used copper clamps [15]. The current was held constant with a DC current power supply at 10A.

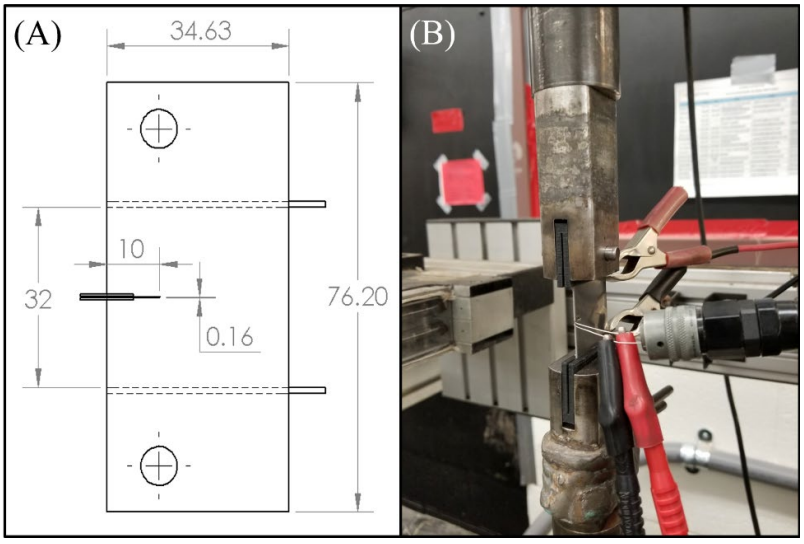

Fig 1 *– (A) Schematic of Fatigue Specimen which shows the EDM cut thickness and length, two pin holes for loading, and the location of the wires. (B) Setup of Fatigue Test showing the two large clamps in the back which provide the 10 amps and the two smaller alligator clips that measure the voltage change.*

Machine Setup

The fatigue crack-growth testing is done on an MTS 810 hydraulic load frame. A custom fixture was machined to hold the specimen and allow both tension and compression of the sample, see Figure 1B, to mount the specimen into the testing machine. To ensure that the sample was positioned vertically, a 3D printed shim was designed. Rolled pins were used to connect the fixture with the specimen. Data from the experimental devices were collected using the MTS Flextest 40 digital controller, with the sampling rate set to 512Hz. The potential was measured using the strain gauge amplifier built into the Flextest hardware. Data was exported as CSV files with a number of cycles, force, and voltage.

Analytical and FEA Comparison

To utilize the voltages taken from the direct current potential drop measurement it is necessary to relate the voltage to a crack length. The relationship between the voltage and crack length is known as a crack length calibration curve. This relationship is a function of not only the geometry of the samples but also the placement of both the current and voltage probes on the specimen. In this study, two methods are employed and compared to derive the calibration curve. The first method is to follow the analytical calibration curve derived by H. Johnson shown in Equation 1. The second method is to use finite element analysis (FEA) to conduct an electrostatic simulation to predict the potential at

the probes with varying crack lengths. The modern approach is to use FEA to derive the calibration curve as it improves the sensitivity at longer crack lengths [15, 16, 17]. Equation 2 is the derived polynomial that describes calibration curved based on the FEA results.

$$\frac{a}{W} = \frac{2}{\pi}\cos^{-1}\left[\frac{\cosh\left(\frac{\pi y}{2W}\right)}{\cosh\left(\frac{V}{V_0}cosh^{-1}\left\{\frac{cosh\left(\frac{\pi y}{2W}\right)}{cos\left(\frac{\pi a_0}{2W}\right)}\right\}\right)}\right] \quad (1)$$

$$\frac{a}{a_0} = 0.0102\left(\frac{V}{V_0}\right)^3 - 0.1787\left(\frac{V}{V_0}\right)^2 + 1.1917\left(\frac{V}{V_0}\right) - 0.02 \quad (2)$$

In Equation 1 and 2, a_0 is the initial crack length (10mm) created by the EDM cut, a is the total crack length, W is the specimen width, y is the plate thickness, V_0 is the initial voltage before crack propagation, and V is the measured voltage throughout the experiment. The result of both of these calibration curves is plotted in Figure 2. There is high accuracy at short crack lengths (the length scale that this study covers) and good agreement between the analytical and FEA calibration curves. It has been elaborated in other studies [16] that FEA calibration has less error than the analytical calibration curve at longer crack lengths. For the remainder of this study, we will use the FEA derived calibration curve.

Because the stress intensity factor is also a function of the geometry it is necessary to account for the sample geometry when predicting the stress intensity factor. There are several closed formed expression that uses empirical geometry correction factors. In this study, an empirical expression for an edge crack under uniaxial stress [18] was considered. The corresponding stress intensity was calculated using the following expression,

$$K_I = \sigma\sqrt{\pi a} * \left[1.122 - 0.231\left(\frac{a}{w}\right) + 10.55\left(\frac{a}{w}\right)^2 - 21.71\left(\frac{a}{w}\right)^3 + 30.382\left(\frac{a}{w}\right)^4\right], \quad (3)$$

where σ is the uniform stress state and the factor rightmost polynomial is a geometrical factor.

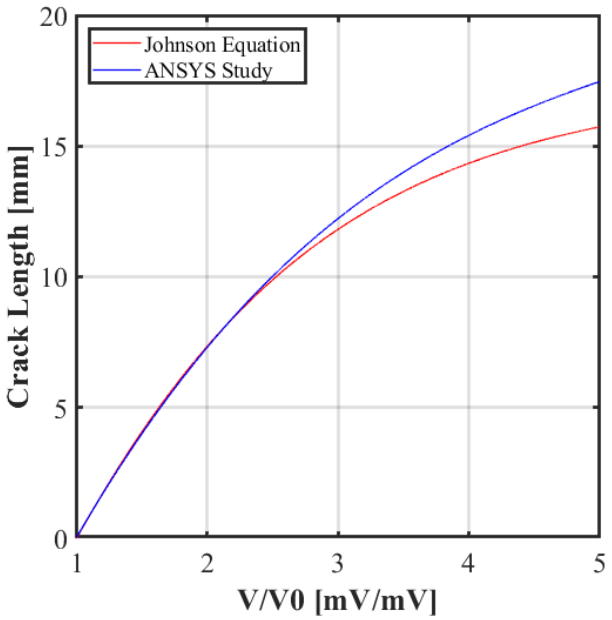

Figure 2 – Plot of the Johnson Analytical Calibration Curve Compared to FEA Derived Curve which shows good agreement between analytical and simulation.

Material Properties

To determine the mechanical properties of the samples an ASTM standard tensile samples were cut out and tested in a tensile machine [18]. The tensile specimen was cut using a plasma cutter the resulting stress-strain curve can be seen in Figure 7 in the appendix. This test gives the Inconel sheet an ultimate tensile strength of 770 MPa at 21% elongation and yield strength of 430 MPa with a modulus of elasticity of 185.4 GPa. Hardness testing was also done with a hardness testing machine which gave a Rockwell-C hardness of 21.1. The hardness values measured show good agreement with cold-rolled plate IN718.

Test Parameters

The specimens were placed in the hydraulic testing machine using pin joints as shown in Figure 1B. Because of the thin design of the specimen, small 3D printed shims were used to align the sample and mitigate tear-out. Because the study is interested in the crack initiation, the specimens did not undergo a crack initiation procedure. In other studies, this is typically done to speed up the initiation of the crack by running at higher stress intensity without a hold cycle to initiate the crack. In this study after the sample was loaded in the machine, data acquisition began with a

loading cycle that was used were made up of two parts, 10 fast oscillations for 30 seconds at a given peak load and that cycled with a ratio between the max and min of R=0.05. Following the oscillation, a 100-second hold with loading at the peak load was carried out. For this study, the peak loads were selected as 1000N, 1200N, 1400N, 1600N, 1700N, and 1800N. More emphasis is given to the three highest loadings. The representative loading cycles as a function of time can be seen in Figure 2. It should be pointed out that the target loading ratio (R=0.05) was specified so that there is a small difference between the true min-max range for the oscillations, as shown in Table 1 below. The actual ratio for all the cases was R=15%. This was a limitation of the control software and inertia of the machine to precisely achieve both the theoretical min and max values.

	Theo. Osc. Min (N)	*Theo. Osc. Max (N)*	*Theo. Osc R (N/N)*	*Act. Osc Min (N)*	*Act. Osc. Max (N)*	*Act. Osc. R(N/N)*
1000N	50	1000	0.05	125	940	0.13
1200N	60	1200	0.05	125	1115	0.11
1400N	70	1400	0.05	180	1310	0.14
1600N	85	1600	0.05	210	1430	0.15
1700N	90	1700	0.05	230	1570	0.15
1800N	95	1800	0.05	250	1630	0.15

Table 1 – Summary of the theoretical and actual min and max forces specified for fatigue cycles. The actual ratio realized by the experiment was R=0.15.

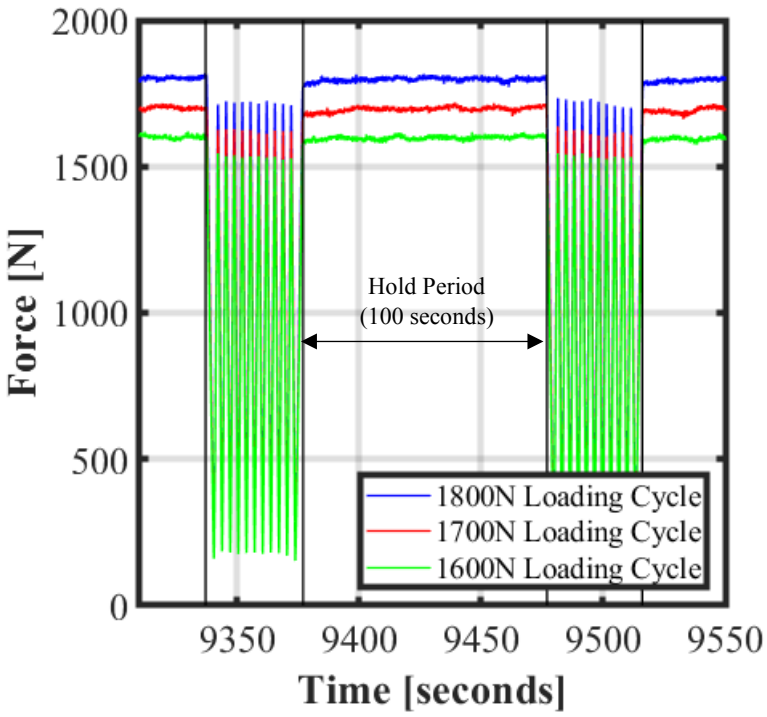

Figure 3 – Plot of the transient loading cycles for three loading cases. One cycle consisted of 10 oscillations between F_{max} and $R*F_{max}$ over a thirty second period, followed by a 100 second hold at F_{max}.

Data Processing

Data acquisition was conducted at a high sampling rate of 512Hz (~2ms/sample) to capture the crack jumps that occur at small length scales and small durations. The data collected was post-processed using Python. To correlate the measured potentials to crack lengths the aforementioned calibration curves were employed along with the stress intensity factor relationship, see the previous section for details. For the 1800N peak load case 18 tests were conducted, for 1700N and 1600N loading cases 22 tests were conducted and 3 tests for 1400N. The data was post-processed by examining the 100-second hold cycles and computing the difference between the crack length over subsequent hold cycles. The difference in crack length between subsequent hold cycles is considered a jump off the crack. For this study, the exact time of occurrence during the hold cycle was not of interest but rather just the quantity and statistics of jumps between subsequent steps. That being said, information about the exact time to the nearest +/-1ms during the hold cycle is available but beyond the scope of the current work.

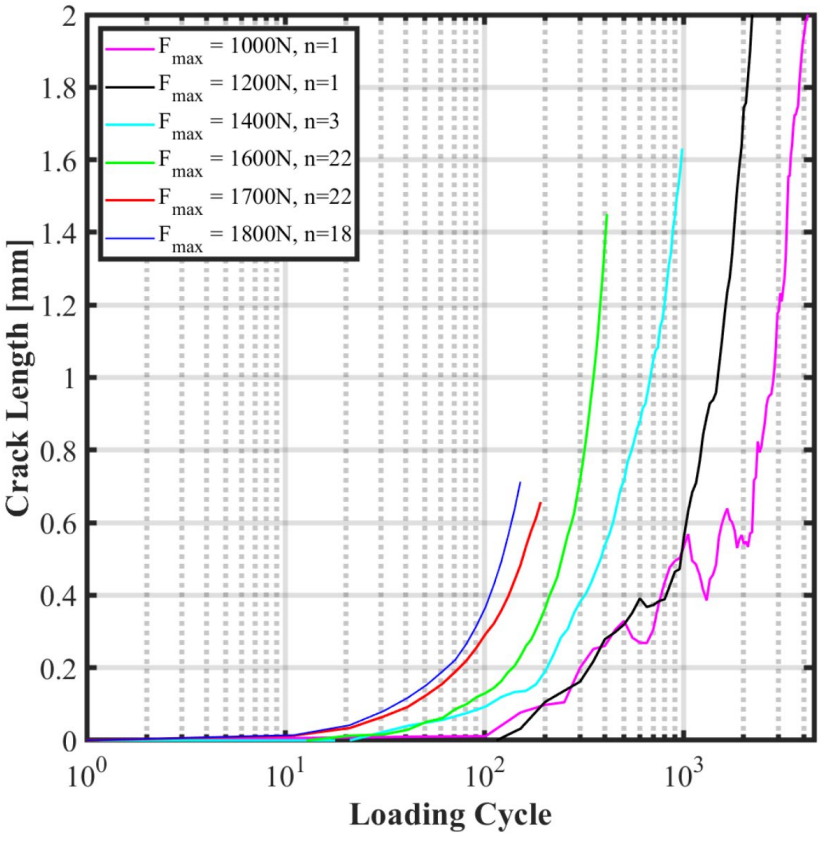

Figure 4 - Average crack length vs. loading cycle number. The test was stopped prior to Region III. Lines are associated with different peak loads or initial stress intensities. Crack length values does not include initial crack length (10mm).

An aspect inherent to this DCPC experimental measurement method is the incorporation of electrical noise in the measurement. This electrical noise is a product of the environment and was minimized by using condition DC power supplies. It is important to point out that the electrical noise in the experiment is random noise. By plotting a histogram of the noise, it was found that the electrical noise is indeed random and follows a normal distribution. This is an important claim because the non-random noise in the DCPC measurement signal is, therefore, a result of some attribute in the system, more specifically, the crack.

Results and Discussion:

Following the experimental procedure outlined above the average crack length for each subsequent holding, cycle was calculated. It should be clarified for the discussion that the terms crack and crack length refer to the crack originating at the end of 10mm EDM cut. Figure 4 is a semi-log plot that illustrates the crack length as a function of cycle number. All tests were stopped prior to Region III. Figure 4 illustrates crack and initiation and growth from

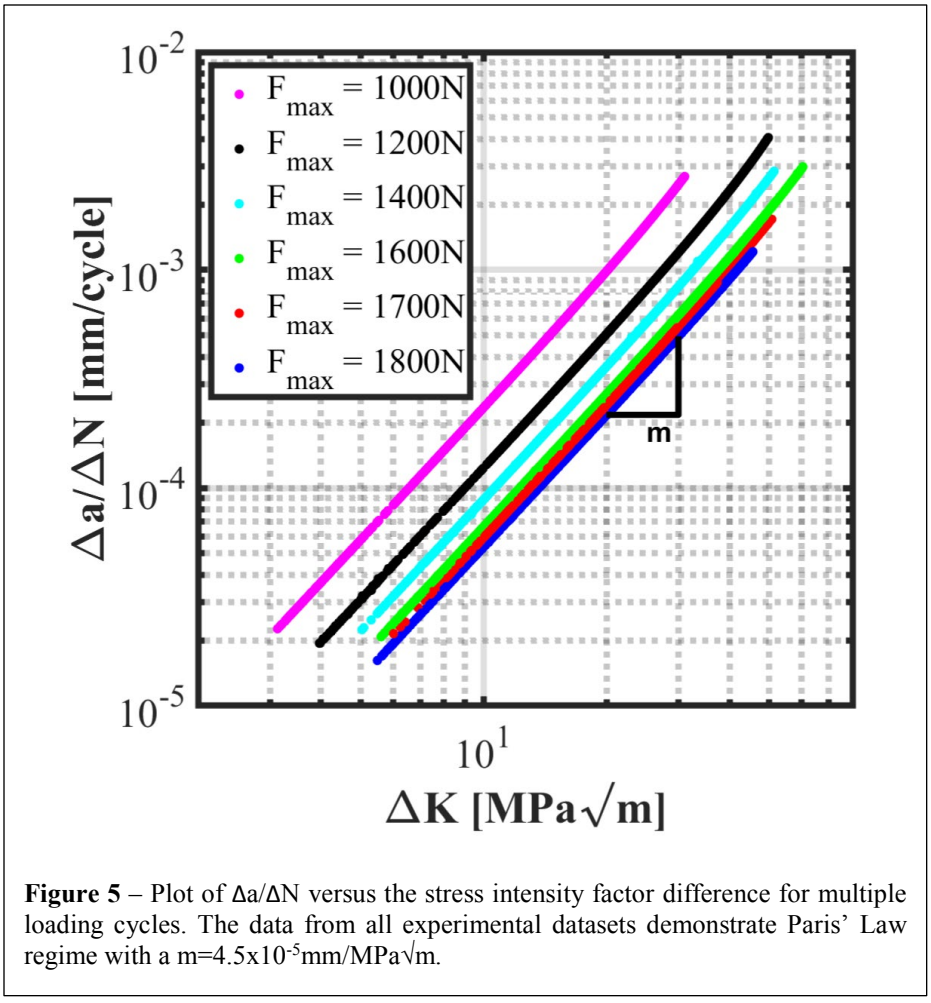

Figure 5 – Plot of Δa/ΔN versus the stress intensity factor difference for multiple loading cycles. The data from all experimental datasets demonstrate Paris' Law regime with a m=4.5x10^{-5}mm/MPa$\sqrt{m}$.

Region I through Region II. The values in the key of Figure 4 correspond to the peak loading values, which can be related to the initial stress intensity. As expected, as the peak load increases the stress intensity increases and the rate of crack propagation will increase. It should be noted, in Figure 4, that the samples were not crack initiated and it takes an increasing about of wall time or cycles depending on the loading to initiate the crack. This is seen as a translation of the curves in the x-axis of Figure 4 and an associated delay in lift-off from the x-intercept. To provide some context to the wall time required for all the cases, the 1800N case took approximately 6.5 hours to reach a crack length of 0.7mm, while 1000N took 72 hours to achieve a similar crack length. This range of time over all the loads considered is still within the low cycle fatigue regium associated with changes in the crack length of mm/hour.

Taking the information from Figure 4 and casting the data in the form of rate of crack length versus stress intensity it is possible to determine which regime of fracture the crack is predominantly undergoing. All samples tested

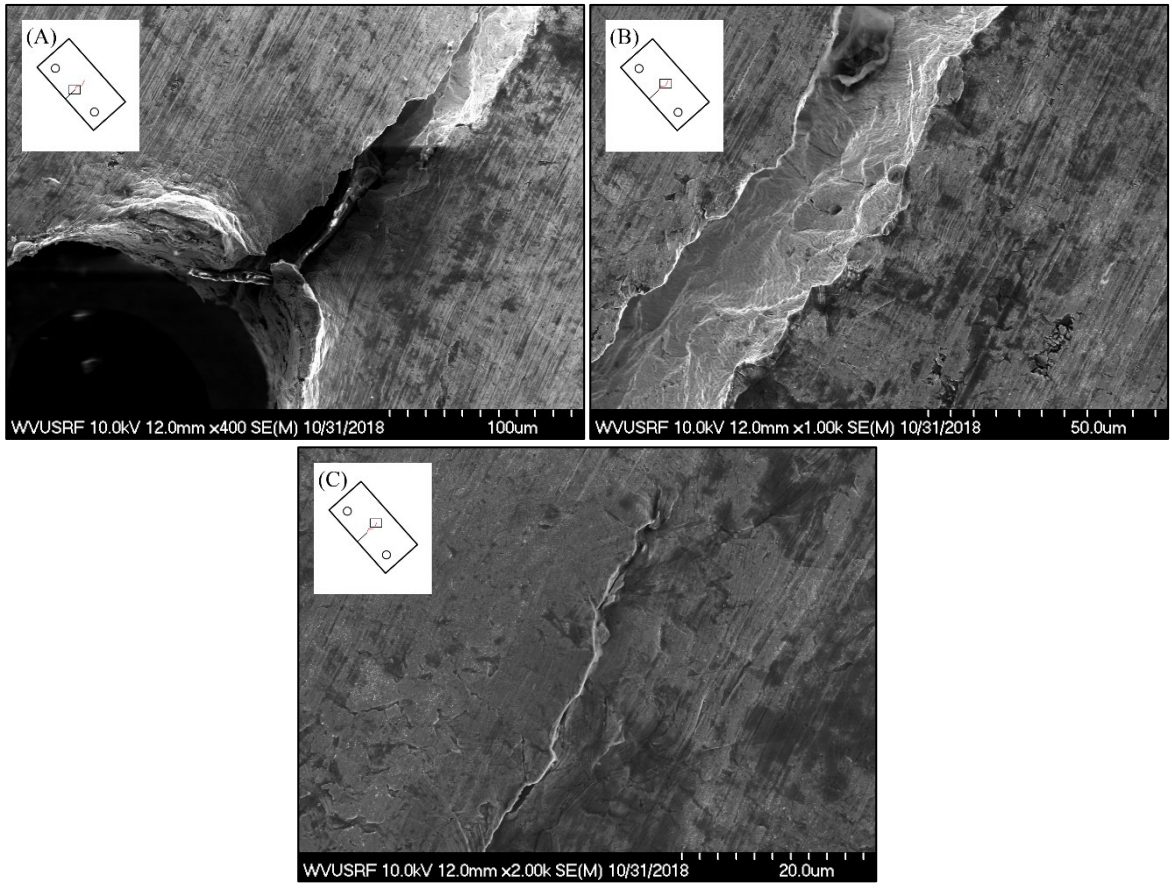

Figure 6 - (A) Crack initiation point showing crack initiation at the back of the EDM cut. (B) Zoomed in image along the crack path at mid-length with visible beach marks with frequecy of 1µm. (C) Termination zone of crack which shows evidance of slip bands at the very tip.

appear to spend the majority of the experiment time in Region II, the Paris Law region [19], while the test was stopped prior to Region III [20]. Figure 5 illustrates the linear nature of the Paris Law for all samples [21] with the corresponding sloped labeled on the figure. Less time was spent in Region I due to the design of the specimen and the position of the load line relative to the EDM cut.

SEM Imaging and Analysis

Scanning Electron Microscopy (SEM) images were taken of the samples after the fatigue tests were completed. Figure 6 is a collection of images from a single specimen with a peak load of 1800N. Figure 6a illustrates that the crack had initiated at the back of the notch that was created by the EDM cut. This is the expected and desirable position of the crack and confirms that the samples are being loaded symmetrically. Figure 6b is an image of the crack at the mid-section of the crack. Looking at the crack surface there is the presence of striations or beach lines, which is synonymous with fatigue [22]. Further examination of the striations reveals that the 1μm+/-0.05μm, which is on the order of the Δa measured using the DCPC reported in Figure 4 and 5. Figure 6b also depicts that the fracture surface is not smooth, which is representative of a more ductile fracture as opposed to a brittle fracture.

Figure 6c is an SEM image at the crack termination prior to Region III for a 1800N case. The extent of crack at stoppage was approximately 0.7mm. From Figure 6c there is evidence of persistent slip bands (PSB) near the crack tip, which are directed away from the crack tip. Typically, during crack initiation, the crack will run along with the plane of the PSB and during crack propagation the PSBs position ahead of the crack in the plastic zone. It can be seen from Figure 6c that the PSB are ahead of the crack tip and therefore it can be visually confirmed by the relative orientation of the PSB that the crack is beyond the initiation phase when the loading is stopped. More interesting is the extent of the plastic zone on either side of the crack extends approximately 8um to either side. Further investigation of the band's width reveals that they are on the order of 0.5μm, which is similar in magnitude to the beach marks found in Figure 6b. It is not obvious how these PSB influence the electric field around the tip, which is an area of future investigation.

Noise Qualification and Quantification

A critical aspect of this study was to qualify and quantify the noise of the crack during fatigue. As mentioned previously, random electrical noise is present from the DCPD method and it is the non-random noise that is of interest. It is expected for a truly random event such as electrical fluctuations from the DCPD method that the distribution

should follow a Gaussian distribution that is centered about a zero mean provided the systematic bias has been removed through calibration. To account for the increase in stress intensity as the crack length increases it was necessary to normalize the change in crack length by the stress intensity for each case. Figure 7 is a plot of the resulting formalized crack length as both a function of the cycle and in a histogram. The rightmost figures of Figure 7a for 1800N and Figure 7b for 1700N is a plot of the normalized crack length as a function of the cycle. If the plots are not normalized by the stress intensity factor there would an increasing trend because the magnitude of the crack length increases as the stress intensity factor increases. As seen in Figure 7a and b there is a definite shift in the from the non-

zero Gaussian mean. Moreover, the magnitude of this shift is greater for higher loading or initial stress intensities. This confirms the claim that cracks make larger jumps when with higher loading or initial stress intensity.

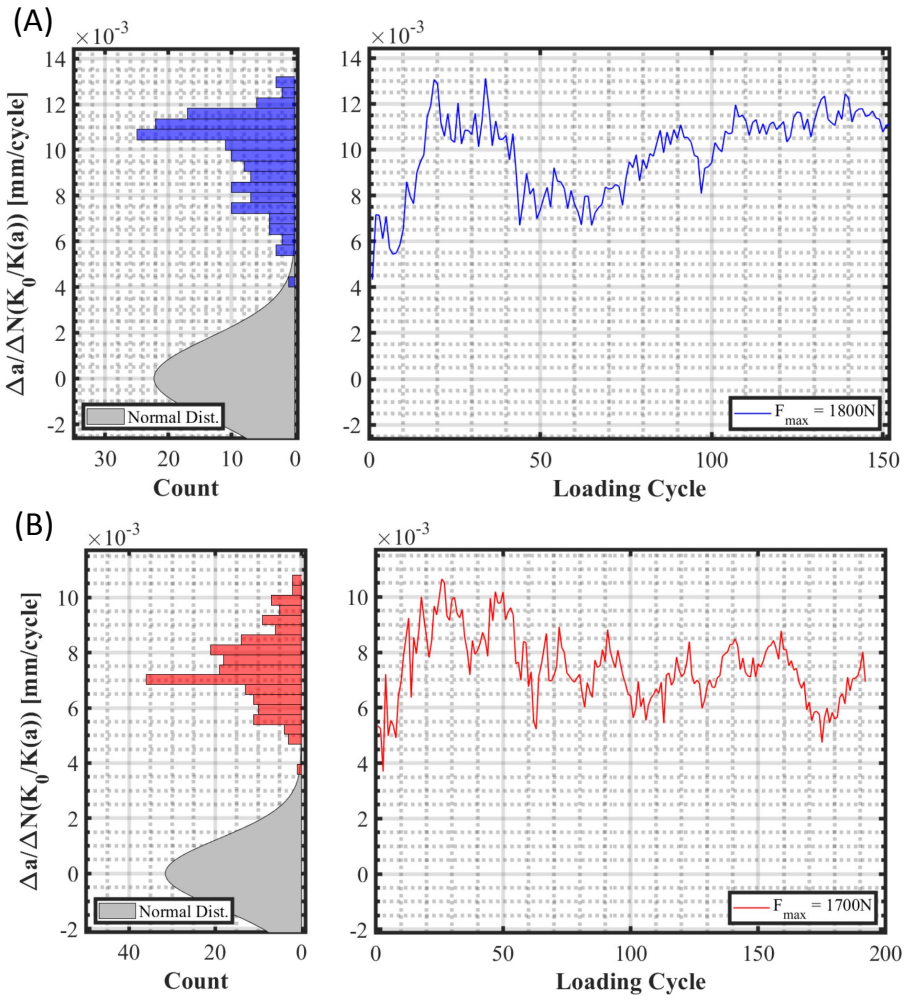

Figure 7 – The rightmost figure are a plot of the normalized crack jumps over subsequent hold cycles. (A) F_{max}=1800N and (B) F_{max}=1700N. The leftmost figures are a histogram of the crack jumps.

Figure 8 is a plot of the relative probability distribution ($v_i = c_i/N$, v_i is bin value, c_i is the count, and N is total number of elements) with data taken from the leftmost subfigures of Figure 7 in addition to additional loading

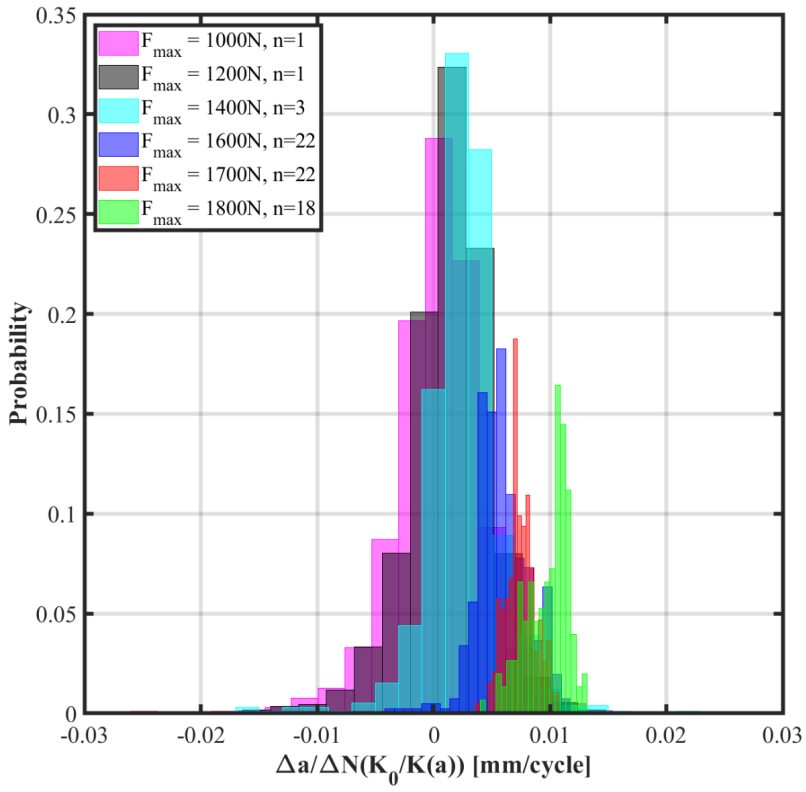

Figure 8 – Relative probability distribution for loading cycles ranging from 1000 to 1800N versus normalized Δa/ΔN. Increasing peak load results in increased magnitude in jumps and decrease in distribution range.

cases. Figure 8 further illustrates the trend that for increased loading there is increased magnitude in the crack jumps. Moreover, Figure 8 provides not only a relative reference to other loadings but also to zero. Comparing the range to each of the other distributions, as the loading increases the range distribution decreases. Additionally, as the peak loading decreases below 1600N there are an appreciable number of negative length crack jumps. While these negative crack length can be reasoned by the crack closure this most likely not the case because the minimum loads are never zero and therefore the crack should not close. The most reasonable explanation of the negative values is that at lower loading the noise associated with the electrical measurement is dominating and the distribution is becoming Gaussian. Another way to explaining this is in terms of the signal-to-noise ratio and the fact that the ratio is decreasing for

decreasing load. This is an important finding in that it provides a discrete cut-off for the signal-to-noise ratio of the proposed DCPD method.

By capturing the statistical variation of the crack jumps for different loading cycle provides a basis of data to be used in more complex simulations. More specifically the rightmost figure of Figure 7 provides a large quantity of data down to the millisecond that is not trivial by plotting the data from the perspective of a probability distribution. However, what the probability distribution of Figure 8 conveys is that there is noise that is statistically non-random that can be trained by data mining techniques. Moreover, and a complementary study to these findings is to use and develop new damage models in phase fields approaches to reproduces these statistical variations and correlate it to materials parameters.

Conclusion:

This study focused on conducting a DCPD measurement on Inconel 718 samples at several peak loads. The crack length was monitored over subsequent hold cycles and a histogram of the normalized crack length jumps was plotted. Several notable trends were apparent from the histograms. First the mean crack length increases with increases loading, second the range of the distribution decreases with increasing load, lastly, the signal-to-noise ratio approaches at a threshold below 1600N for the described setup. The most significant finding was that there is non-random statistical features in the crack length jumps that have the potential to identify and correlate with material attributes using machine learning approaches.

References:

[1] K. G. Kyprianidis, "Future Aero Engine Designs: An Evolving Vision," in *Advances in Gas Turbine Technology*, IntechOpen, 2011.

[2] S. Farokhi, Aircraft Propulsion, Chichester (UK): John Wiley & Sons, 2014.

[3] J. P. Downs and K. K. Landis, "Turbine Cooling Systems Design: Past, Present and Future," in *ASME Turbo Expo 2009: Power for Land, Sea, and Air*, Orlando, 2009.

[4] R. Reed, "The Minerals, Metals & Materials Society (TMS)," February 2007. [Online]. Available: https://www.tms.org/Communities/FTAttachments/Superalloys%20Applications%20Primer.pdf.

[5] Special Metals, "INCONEL® Alloy 718," 2007. [Online]. Available: http://www.specialmetals.com/assets/smc/documents/alloys/inconel/inconel-alloy-718.pdf.

[6] S. J. Hong, W. P. Chen and T. W. Wang, "A diffraction study of the γ ″phase in INCONEL 718 superalloy," *Metallurgical and Materials Transactions A,* vol. 32, no. 8, pp. 1887-1901, 2001.

[7] C. Slama and M. Abdellaoui, "Structural characterization of the aged Inconel 718," *Journal of alloys and compounds,* vol. 306, no. 1-2, pp. 277-284, 2000.

[8] M. W. Davidson, "MicroscopyU," Nikon, [Online]. Available: https://www.microscopyu.com/microscopy-basics/resolution.

[9] D. Chen, C. J. Gilbert and R. O. Ritchie, "In Situ Measurement of Fatigue Crack Growth Rates in a Silicon Carbide Ceramic at Elevated Temperatures Using a DC Potential System," *Journal of Testing and Evaluation,* vol. 28, no. 4, pp. 236-241, 2000.

[10] W. Zhang and Y. Liu, "Investigation of incremental fatigue crack growth mechanisms using in situ SEM testing," *International Journal of Fatigue,* vol. 42, pp. 14-23, 2011.

[11] C. Roux-Langlois, A. Gravouil, M. C. Baietto, J. Rethore, F. Mathieu, F. Hild and S. Roux, "DIC identification and X-FEM simulation of fatigue crack growth basedon the Williams' series," *International Journal of Solids and Structures,* vol. 53, pp. 38-47, 2015.

[12] S. Roux, J. Rethore and F. Hild, "Digital Image Correlation and Fracture: An Advanced Technique for Estimating Stress Intensity Factors of 2D and 3D Cracks," *Journal of Physics D: Applied Physics,* vol. 42, 2009.

[13] J. D. Carrol, W. Abuzaid, J. Lambros and H. Sehito, "High resolution digital image correlation measurements of strain accumulation in fatigue crack growth," *International Journal of Fatigue,* vol. 57, pp. 140-150, 2013.

[14] ASTM, "E1457-15 Standard Test Method for Measurement of Creep Crack Growth Times in Metals," ASTM, 2015. [Online]. Available: https://www.astm.org/Standards/E1457.htm. [Accessed 1 February 2019].

[15] H. H. Johnson, "Calibrating the Electric Potential Method for Studying Slow Crack Growth," *Materials Research & Standards,* vol. 5, no. 9, p. 442–445, 1965.

[16] K. M. Tarnowski, K. M. Nikbin, D. W. Dean and C. M. Davies, "A Unified Potential Drop Calibration Function for Common Crack Growth Specimens," *Experimental Mechanics,* vol. 58, no. 6, pp. 1003-1013, 2018.

[17] K. Schwalbe and D. Hellmann, "Application of the Electrical Potential Method to Crack Length Measurements Using Johnson's Formula," *Journal of Testing and Evaluation,* vol. 9, no. 3, pp. 218-220, 1981.

[18] ASTM, "E8/E8M-16 Standard Test Methods for Tension Testing of Metallic Materials," ASTM, 2018. [Online]. Available: https://www.astm.org/Standards/E8. [Accessed 1 February 2019].

[19] P. Paris and F. Erdogan, "A Critical Analysis of Crack Propogation Laws," *Journal of Basic Engineering,* vol. 85, no. 4, pp. 528-533, 1963.

[20] R. G. Budynas, J. K. Nisbett and J. E. Shigley, Shigley's mechanical engineering design, New York: McGraw-Hill, 2011.

[21] S. Suresh, Fatigue of Materials, Cambridge University Press, 1998.

[22] J. Ronald, "Fractography of Metals and Plastics," *Plastics Failure Analysis and Prevention,* pp. 127-134, 2001.

Appendix:

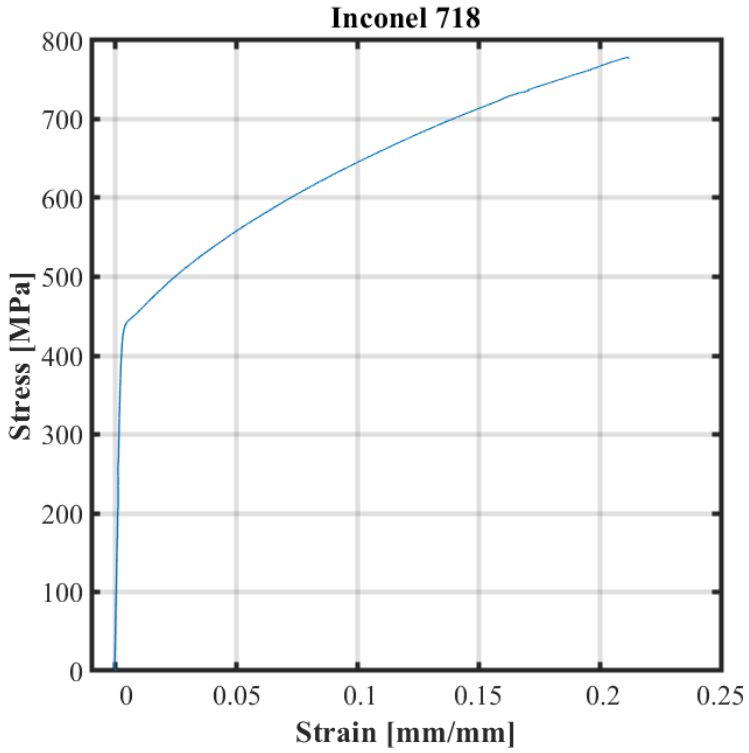

Figure 7 - Experimental Stress Strain Curve for Plate Inconel 718

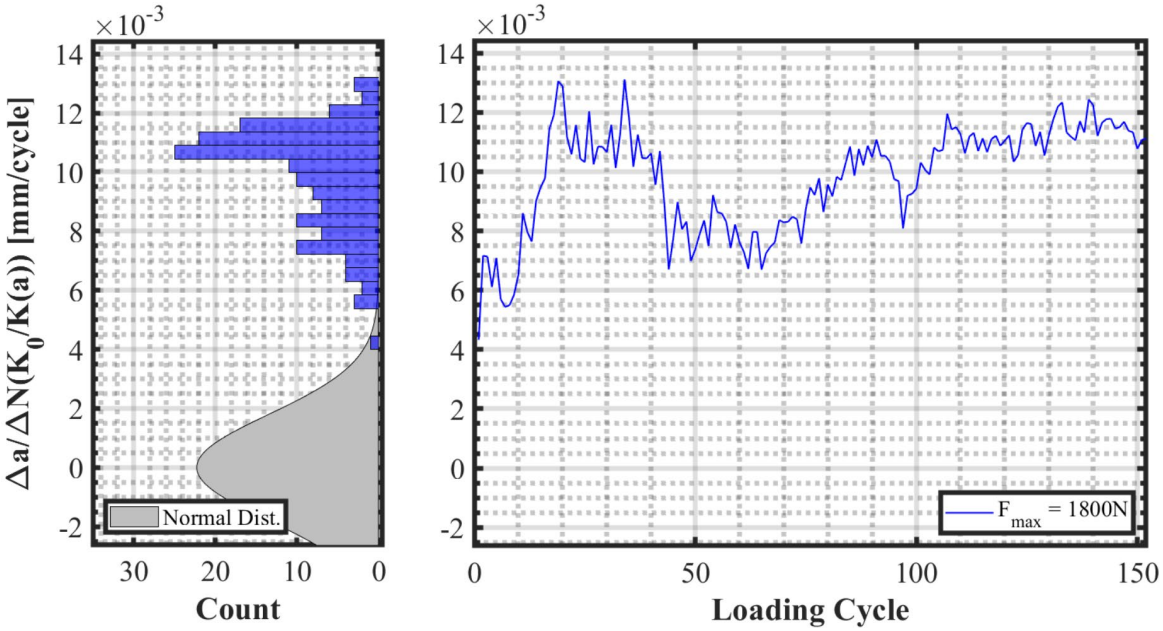

Figure 8 - Normalized Δa/ΔN Noise Plot vs hold Cycle for 1800N Loading and Histogram Spread of Crack Growth Events.

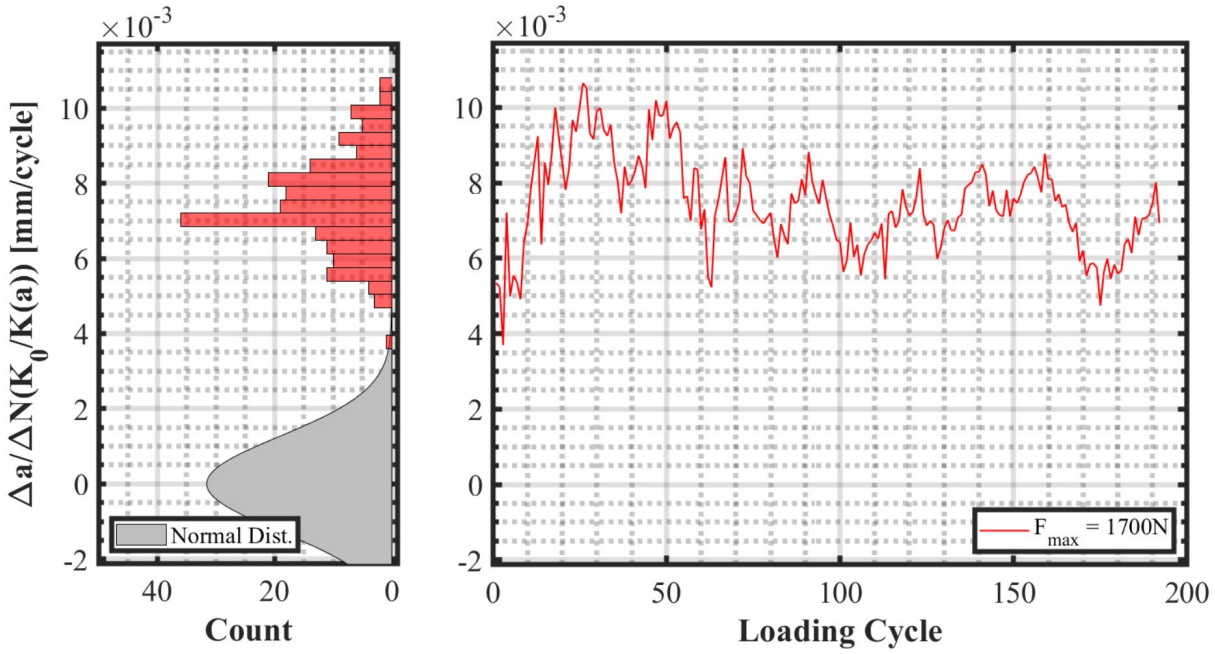

Figure 9 - Normalized Δa/ΔN Noise Plot vs hold Cycle for 1700N Loading and Histogram Spread of Crack Growth Events.

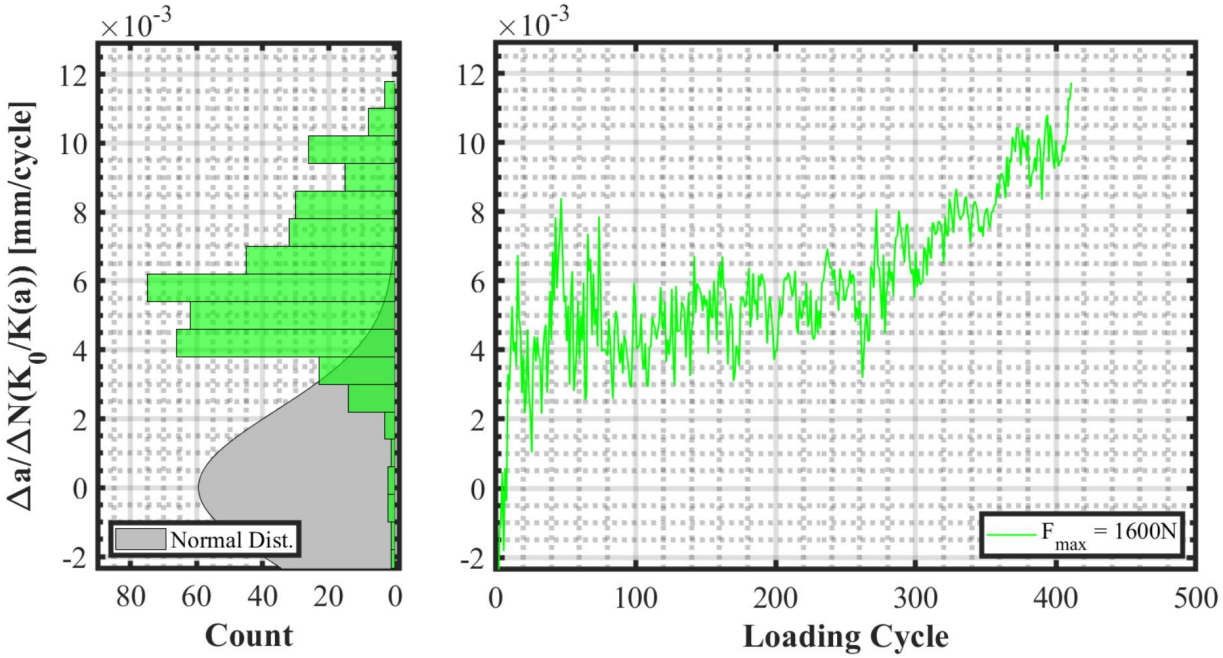

Figure 10 - Normalized Δa/ΔN Noise Plot vs hold Cycle for 1600N Loading and Histogram Spread of Crack Growth Events.

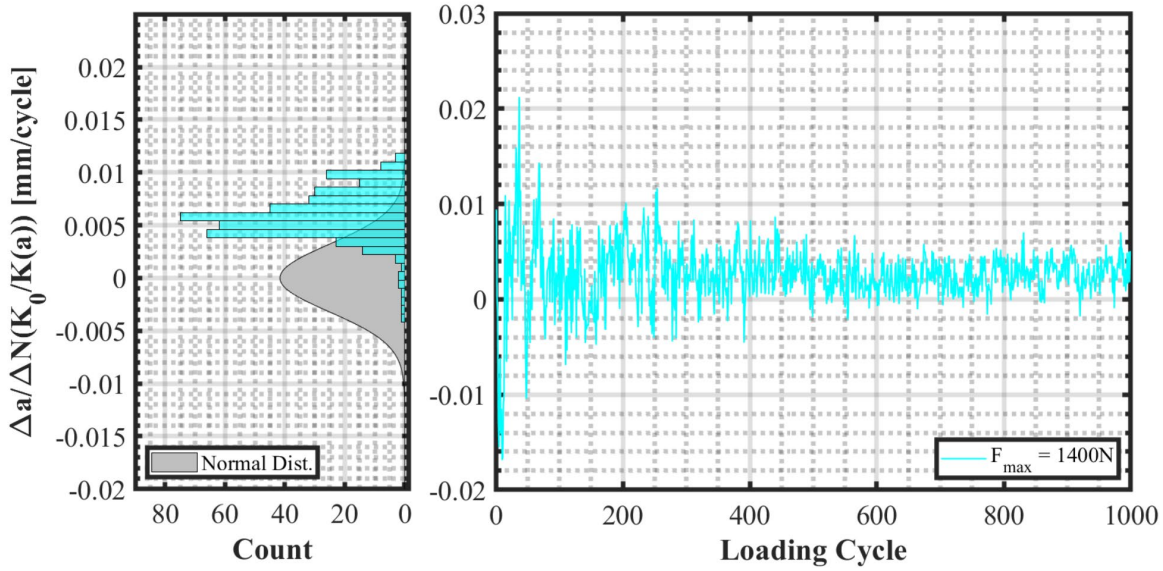

Figure 11 - Normalized Δa/ΔN Noise Plot vs hold Cycle for 1400N Loading and Histogram Spread of Crack Growth Events.

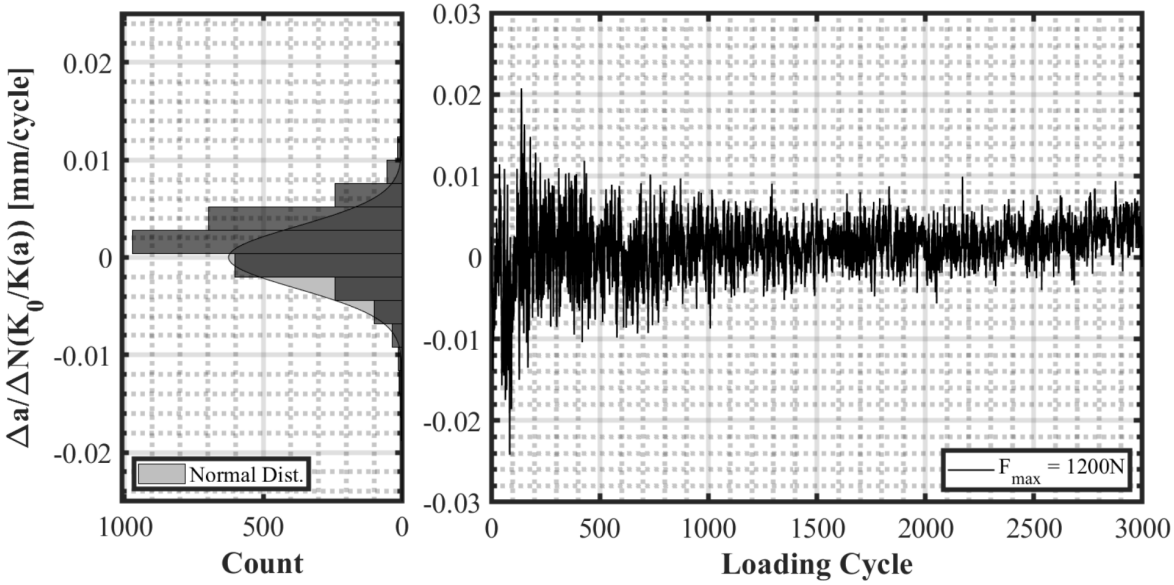

Figure 12 - Normalized Δa/ΔN Noise Plot vs hold Cycle for 1200N Loading and Histogram Spread of Crack Growth Events.

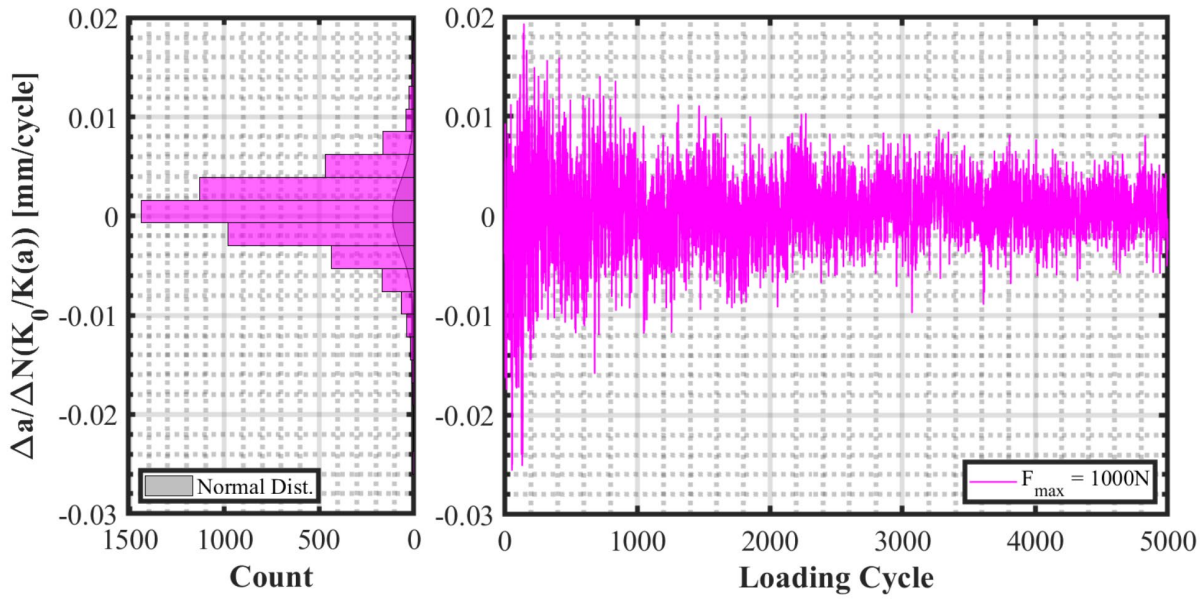

Figure 13 - Normalized Δa/ΔN Noise Plot vs hold Cycle for 1000N Loading and Histogram Spread of Crack Growth Events.